A Density Functional Study of the Mechanism of the Diimine−Nickel-Catalyzed Ethylene Polymerization Reaction

Djamaladdin G. Musaev, Robert D. J. Froese, Mats Svensson, and Keiji Morokuma*

Contribution from the Cherry L. Emerson Center for Scientific Computation and Department of Chemistry, Emory University, Atlanta, Georgia 30322

Received August 13, 1996. Revised Manuscript Received November 1, 1996[⊗]

Abstract: The mechanism of diimine−Ni-catalyzed ethylene polymerization reaction has been studied theoretically using the B3LYP density functional method. The chain initiation reaction proceeds with the coordination of ethylene to the model active catalyst $[L_2NiCH_3]^+$, $L_2 = (HNCH)_2$, followed by ethylene insertion into the metal−alkyl bond with a rate-determining 11.7 kcal/mol free energy barrier to form a γ-agostic intermediate, which with a small barrier rearranges to a more stable β-agostic intermediate and then forms an olefin alkyl complex upon coordination of the next ethylene. Linear polymer propagation takes place from this olefin alkyl complex, the resting state in the catalytic cycle, via the same insertion, rearrangement, and coordination pathway. An alternative pathway from the olefin alkyl complex passes over a 14−15 kcal/mol barrier for β-hydride elimination and reinsertion for branched polymer propagation. These energetics suggest that the Ni(II)-catalyzed reaction is expected to produce more linear than methyl-branched polymers, and that higher temperature increases and higher ethylene pressure decreases the branching. Hydrogenolysis is an energetically favorable termination pathway, proceeding via coordination of a hydrogen molecule to the metal center, followed by H−H activation through a four-centered "metathesis-like" transition state and reductive elimination of alkane. A comparison with zirconocene-catalyzed ethylene polymerization shows that the Ni(II)-catalyzed polymerization should be slightly slower and should give more branching.

I. Introduction

The mechanism of transition metal catalyzed olefin polymerization reactions has been extensively studied by experimentalists[1] and theoreticians[2] during the last decades. These studies have practical and fundamental significance, allowing the control of polymer microstructures and molecular weights and the discovery of new and more efficient catalysts. The main efforts have been concentrated on studies of metallocenes and geometry constrained catalysts of the d^0 and d^0f^n elements.[1] Recently, Brookhart and co-workers[3] have reported new Pd(II)- and Ni(II)-based catalysts for ethylene polymerization. It was shown that the Pd(II) and Ni(II) initiators are cationic methyl complexes $[L_2MMe]^+$ (M = Ni, Pd) having bulky diimine ligands L_2 = ArN═C(R)C(R)═NAr, where Ar = 2,6-$C_6H_3(i\text{-}Pr)_2$ and 2,6-$C_6H_3Me_2$, and R = H and Me**.** Polyethylenes produced by using Pd(II) catalysts show extensive branching along the main chain, randomly distributed and of variable length. Polyethylenes produced by Ni(II) catalysts range from highly linear to moderately branched. The extent of branching is a function of temperature, ethylene pressure, and catalyst structure. Increased branching occurs with higher temperatures and decreased branching occurs at higher ethylene pressures. Reducing the steric bulk of the diimine ligand results in less branched, more linear polymers, with decreased molecular weight. Ni(II) catalysts have been found to be extremely active, comparable to metallocene catalysts. The proposed mechanism of the catalysis,[3] shown in Scheme 1, includes the initiation step via the coordination of olefin to the diiminemetal methyl cation **I**, followed by migratory insertion into the metal−alkyl bond and formation of a new alkyl complex **III**. A second olefin can bind to this species giving the complex **IV**, as shown in path A, and subsequent olefin insertion leads to chain growth and the formation of linear polyethylenes. Alternatively, **III** can eliminate β-hydride to yield 1-alkene hydride complex **VI**. This species can undergo reinsertion with opposite regiochemistry and the production of a branched alkyl ligand, as shown as path B. Further olefin coordination and insertion produce a branched polyethylene. The complex **VI** can associatively or dissociatively displace the branched olefin by ethylene to give **X**, as shown as path C; with this chain transfer, a chain is terminated with the formation of a terminal olefin and a new chain is initiated. The choice of three paths, A, B, and C, exits not only for the initiation intermediate **III** but also for all the diiminemetal alkyl intermediates, such as **V**, **VII**, **IX**, and **XI**, during the polymerization process, and complicated branching patterns in polyethylene can be obtained.

Several key questions in the proposed mechanism remain unclear. (i) What are the structure and the relative energies of reactants, intermediates, transition states, and products of these reactions? (ii) Why is the Ni(II) catalyst more active than Pd(II)? (iii) Why does the Ni(II) catalyst produce more linear

[⊗] Abstract published in *Advance ACS Abstracts,* January 1, 1997.

(1) As leading references, see: (a) Huang, J.; Rempel, G. L. *Prog. Polymer Sci.* **1995**, *20*, 459 and references therein. (b) Coates, G. W.; Waymouth, R. M. *Science* **1995**, *267*, 217. (c) van der Linden, A.; Schaverien, C. J.; Meijboom, N.; Ganter, C.; Orpen, A. G. *J. Am. Chem. Soc.* **1995**, *117*, 3008. (d) Alameddin, N. G.; Ryan, M. F.; Eyler, J. R.; Siedle, A. R.; Richardson, D. E. *Organometallics* **1995**, *14*, 5005 and references therein. (e) Yang, X.; Stern, C. L.; Marks, T. J. *J. Am. Chem. Soc.* **1994**, *116*, 10015. (f) Coughlin, E. B.; Bercaw, J. E. *J. Am. Chem. Soc.* **1992**, *114*, 7606. (g) Crowther, D. J.; Baenziger, N. C.; Jordan, R. F. *J. Am. Chem. Soc.* **1991**, *113*, 1455. (h) Kaminsky, W.; Kulper, K.; Brintzinger, H. H.; Wild, F. R. W. P. *Angew. Chem., Int. Ed. Engl.* **1985**, *24*, 507. (i) Ewen, J. A. *J. Am. Chem. Soc.* **1984**, *106*, 6355.

(2) As leading references, see: (a) Yoshida, T.; Koga, N.; Morokuma, K. *Organometallics* **1995**, *14*, 746. (b) Yoshida, T.; Koga, N.; Morokuma, K. *Organometallics* **1996**, *15*, 766. (c) Woo, T. K.; Fan, L.; Ziegler, T. *Organometallics* **1994**, *13*, 2252. (d) Fan, L.; Harrison, D.; Woo, T. K.; Ziegler, T. *Organometallics* **1995**, *14*, 2018. (e) Hyla-Kryspin, I.; Niu, S.; Gleiter, R. *Organometallics* **1995**, *14*, 964. (f) Fan, L.; Harrison, D.; Deng, L.; Woo, T. K.; Swerhone, D.; Ziegler, T. *Can. J. Chem.* **1995**, *73*, 989. (g) Lohrenz, J. C. W.; Woo, T. K.; Fan, L.; Ziegler, T. *J. Organomet. Chem.* **1995**, *497*, 91.

(3) Johnson, L. K.; Killian, C. M.; Brookhart, M. *J. Am. Chem. Soc.* **1995**, *117*, 6414.

S0002-7863(96)02831-4 CCC: $14.00

Scheme 1. Proposed Mechanism of the Pd(II) and Ni(II)-Catalyzed Ethylene Polymerization Reaction

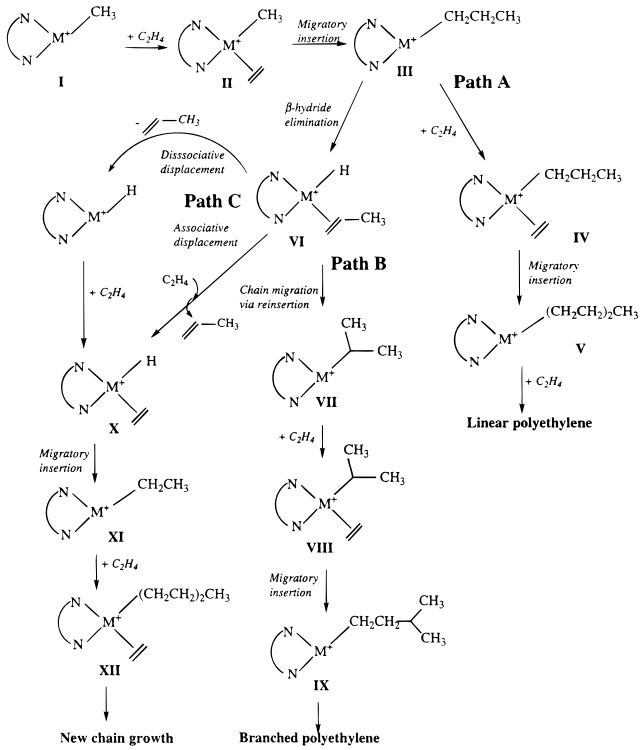

polymers than Pd(II)? (iv) What factors, electronic or steric, are responsible for giving branched polymers? (v) What is the difference in the mechanism between metallocene- catalyzed polymerization and the present M(II)-catalyzed polymerization? (vi) What is the dominant chain termination step, and how can the weight of the polymers be controlled?

In order to provide some answers to these questions, quantum chemical calculations will be performed to find critical structures and their energies on the potential energy surface for the following reaction steps (where M = Pd and Ni).

Chain initiation (olefin coordination and insertion to the active catalyst):

$$[L_2M(CH_3)]^+ + CH_2{=}CH_2 \rightarrow [L_2M(CH_2CH_2CH_3)]^+ \quad (1)$$

Chain propagation—path A (olefin coordination and insertion giving a linear polymer growth):

$$[L_2M(CH_2CH_2CH_3)]^+ + CH_2{=}CH_2 \rightarrow [L_2M((CH_2CH_2)_2CH_3)]^+ \quad (2)$$

Chain propagation—path B (β-hydride elimination and olefin reinsertion giving a branched polymer growth):

$$[L_2M(CH_2CH_2CH_3)]^+ \rightarrow [L_2M(H)(CH_2{=}CHCH_3)]^+ \rightarrow [L_2M(CH(CH_3)_2)]^+ + CH_2{=}CH_2 \rightarrow [L_2M(CH_2CH_2CH(CH_3)_2)]^+ \quad (3)$$

Chain termination or chain transfer (β-hydride elimination and olefin dissociation):

$$[L_2M(CH_2CH_2CH_3)]^+ \rightarrow [L_2M(H)(CH_2{=}CHCH_3)]^+ \rightarrow [L_2MH]^+ + CH_2{=}CHCH_3 \quad (4)$$

Chain termination or chain transfer (hydrogenolysis):

$$[L_2M(CH_2CH_2CH_3)]^+ + H_2 \rightarrow [L_2M(H_2)(CH_2CH_2CH_3)]^+ \rightarrow [L_2MH]^+ + CH_3CH_2CH_3 \quad (5)$$

L_2 is the model diimine HN=C(H)C(H)=NH we have adopted in the present paper, and the abbreviation L_2 will be used through the paper for this ligand.

This paper is part of a series of studies on catalytic cycles involving diimine complexes. We have already studied[4] the potential energy surfaces for copolymerization of ethylene and carbon monoxide catalyzed by $[L_2MCH_3]^+$ (M = Pd and Ni), where L_2 is the same model diimine as used above. In the present paper, we will examine the mechanism of reactions 1−5 for M = Ni, and compare the results with those for zirconocene-based catalysts. In a separate paper,[5] the corresponding reactions 1−5 for M = Pd will be studied and compared with the results for M = Ni. In the future, we plan to use the recently developed IMOMM (Integrated Molecular Orbital + Molecular Mechanics) and IMOMO methods[6] to study the effects of the bulky substituents on the reaction mechanism.

II. Calculation Procedure

Geometries and energies of the reactants, intermediates, transition states, and products of reactions 1−5 are calculated using the gradient-corrected density functional theory B3LYP,[7] which has been shown to be quite reliable both in geometry and in energy.[8] In these calculations we used the LANL2DZ basis set which includes a double-ζ valence basis set[9] (8s5p5d)/[3s3p2d] for Ni with the Hay and Wadt ECP replacing core electrons up to 2p and the Huzinaga−Dunning double-ζ quality basis set[10] for the active part, i.e., C and H atoms of alkyl groups and olefins, while the standard 3-21G basis set[11] was adopted for N, C, and H atoms of the HN=C(H)C(H)=NH ligand. All intermediate and transition state structures were optimized without any symmetry constraints. Systematic vibrational analysis was carried out for identification of the number of imaginary frequencies and determination of zero-point energy and Gibbs free energy only for some important intermediates and the migratory insertion transition state of the chain initiation reaction (1). All calculation have been performed by the

(4) Svensson, M.; Matsubara, T.; Morokuma, K. *Organometallics* **1996**, *15*, 5568.
(5) Musaev, D. G.; Svensson, M.; Morokuma, K. ; Siegbahn, P. E. M. *Organometallics*, submitted for publication.
(6) (a) Maseras, F.; Morokuma, K. *J. Comput. Chem.* **1995**, *16*, 1170. (b) Matsubara, T.; Maseras, F.; Koga, N.; Morokuma, K. *J. Phys. Chem.* **1996**, *100*, 2573. (c) Humbel S.; Sieber, S.; Morokuma, K., *J. Chem. Phys.* **1996**, *105*, 1959.
(7) (a) Becke, A. D. *Phys. Rev. A* **1988**, *38*, 3098. (b) Lee, C.; Yang, W.; Parr, R. G. *Phys. Rev. B* **1988**, *37*, 785. (c) Becke, A. D. *J. Chem. Phys.* **1993**, *98*, 5648.
(8) (a) Musaev, D. G.; Morokuma, K. *J. Phys. Chem.* **1996**, *100*, 6509. (b) Erikson, L. A.; Pettersson, L. G. M.; Siegbahn, P. E. M.; Wahlgren, U. *J. Chem. Phys.* **1995**, *102*, 872. (c) Ricca, A.; Bauschlicher, C. W., Jr. *J. Phys. Chem.* **1994**, *98*, 12899. (d) Heinemann, C.; Hertwig, R. H.; Wesendrup, R.; Koch, W.; Schwarz, H. *J. Am. Chem. Soc.* **1995**, *117*, 495. (e) Hertwig, R. H.; Hrusak, J.; Schroder, D.; Koch, W.; Schwarz, H. *Chem. Phys. Lett.* **1995**, *236*, 194. (f) Schroder, D.; Hrusak, J.; Hertwig, R. H.; Koch, W.; Schwerdtfeger, P.; Schwarz, H. *Organometallics* **1995**, *14*, 312. (g) Fiedler, A.; Schroder, D.; Shaik, S.; Schwarz, H. *J. Am. Chem. Soc.* **1994**, *116*, 10734. (h) Fan, L.; Ziegler, T. *J. Chem. Phys.* **1991**, *95*, 7401. (i) Berces, A.; Ziegler, T.; Fan, L. *J. Phys. Chem.* **1994**, *98*, 1584. (j) Lyne, P. D.; Mingos, D. M. P.; Ziegler, T.; Downs, A. J. *Inorg. Chem.* **1993**, *32*, 4785. (k) Li, J.; Schreckenbach, G.; Ziegler, T. *J. Am. Chem. Soc.* **1995**, *117*, 486.
(9) (a) Hay, P. J.; Wadt, W. R. *J. Chem. Phys.* **1985**, *82*, 299. (b) Wadt, W. R.; Hay, P. J. *J. Chem. Phys.* **1985**, *82*, 284.
(10) (a) Dunning, T. M., Jr. *J. Chem. Phys.* **1971**, *55*, 716. (b) Dunning, T. M., Jr. *J. Chem. Phys.* **1970**, *53*, 2823.
(11) (a) Binkley, J. S.; Pople, J. A.; Hehre, W. J. *J. Am. Chem. Soc.* **1980**, *102*, 939. (b) Gordon, M. S.; Binkley, J. S.; Pople, J. A.; Pietro, W. J.; Hehre, W. J. *J. Am. Chem. Soc.* **1982**, *104*, 2797. (c) Pietro, W. J.; Francl, M. M.; Hehre, W. J.; DeFrees, D. J.; Pople, J. A.; Binkley, J. S. *J. Am. Chem. Soc.* **1982**, *104*, 5039.

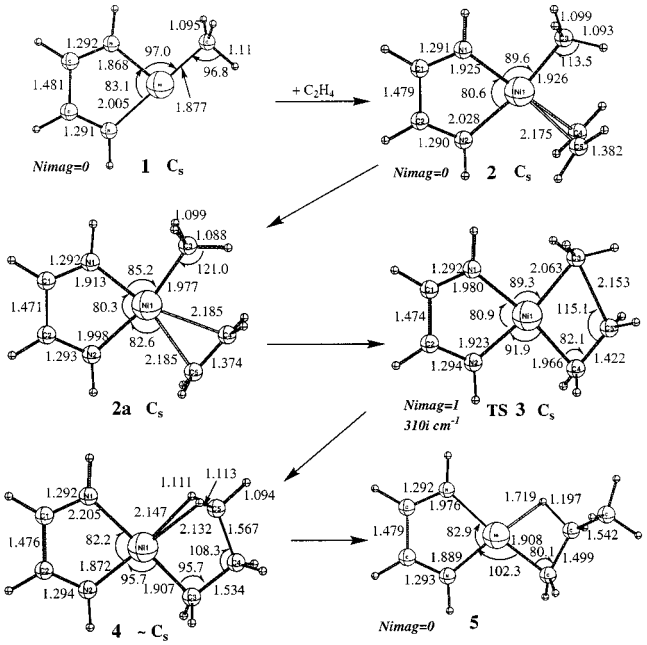

Figure 1. Optimized geometries (in Å and deg) of reactants, transition states, and intermediates of the chain initiation step (1): $[L_2M(CH_3)]^+ + CH_2{=}CH_2 \rightarrow [L_2M(CH_2CH_2CH_3)]^+$. Label C_s indicates that C_1 optimization converged to a C_s structure.

Gaussian94 package,[12] supplemented by our own analytical second derivative code for ECP.[13]

III. Chain Initiation

As suggested by Brookhart,[3] we have assumed the active catalyst initiating reaction (1) to be the cation complex $[L_2MCH_3]^+$ (**1**). As shown in Figure 1, **1** is calculated to be a true minimum with a T-shaped planar (C_s) structure with two Ni−N bond lengths of 1.868 and 2.005 Å. The two Ni−N bond lengths are quite different because of to the *trans* influence of the methyl group. The methyl C−H bond in the C_s plane is longer by 0.017 Å than the other two, indicative of a weak α-agostic interaction with the metal. The initial step of reaction 1 is the coordination of ethylene to the reactant **1**. Two π-complexes, both having C_s symmetry, were found: **2** and **2a** with perpendicular and parallel ethylene, respectively, with respect to the Ni(N=C−C=N) plane. The perpendicular π-complex **2** is the more stable structure and is confirmed to be a real minimum. The parallel complex **2a** lies 6.3 kcal/mol above **2**, as shown in Table 1, presumably because of the larger steric repulsion. Though we did not fully optimize the structure of the rotational transition state, the barrier from **2a** is very small. Both $Ni-C^{olefin}$ distances in **2** are 2.185 Å, vs the 1.85−1.95 Å values in typical Ni−C σ-bonds.[14] The olefin is slightly activated as the bond length of 1.382 Å in **2** is stretched by 0.034 Å from 1.348 Å in free ethylene. The two Ni−N bond lengths are stretched relative to the reactant, from 1.868 to 1.926 Å and 2.005 to 2.028 Å. The binding energies of ethylene for the π-complex **2** are 27.9 and 25.5 kcal/mol calculated using total energy without and with the zero-point correction, respectively, as shown in Table 1. Owing to the entropy contribution, the Gibbs free energy for this bonding at 298.15 K, 14.9 kcal/mol, is about half that calculated using only the potential energy.

From the π-complex **2**, the reaction proceeds through the transition state **3** with C_s symmetry to the γ-agostic propyl complex **4**. It is expected that the path of the reaction passed near the vicinity of the parallel complex **2a**. The Hessian analysis confirms that **3** is a transition state with one imaginary frequency of 310i corresponding to the insertion of ethylene into the Ni−CH_3 bond. This migratory insertion step results in the breaking of a Ni−C bond and a Ni−C_2H_4 interaction and the forming of new Ni−C and C−C bonds. The C−C bond length increases from 1.382 Å in the π-complex to 1.422 Å in the transition state to 1.534 Å in the γ-agostic product. This γ-agostic product **4** has nearly C_s symmetry with a slightly rotated γ-methyl group. Two C−H bonds are involved in the

Table 1. Total Energies (in au) of Reactants and Relative Energies (in kcal/mol) of the Intermediates, Transition States, and Products of Reactions 1−5, at the B3LYP Level

structure	label	energy
Reactants		
H_2		−1.174418
CH_4		−40.514469
$CH_2{=}CH_2$		−78.578208
$CH_2{=}CHCH_3$		−117.891289
$CH_3CH_2CH_3$		−119.125552
$[L_2NiCH_3]^+$	**1**	−396.057706
$[L_2NiH]^+$	**19**	−356.724179
Chain Initiation: (Reaction 1)		
$[L_2NiCH_3]^+ + 2\ CH_2{=}CH_2$		0.0
perpendicular π-complex	**2**	−27.9/−25.5//−14.9[a]
parallel π-complex	**2a**	−21.6
insertion transition state	**3**	−18.0/−14.8//−3.2
γ-agostic *n*-propyl product	**4**	−33.3
β-agostic *n*-propyl product	**5**	−39.3(0.0)[b]/−35.4// −24.2
Chain Propagation: Path A: (Reaction 2)		
π-Complex	**6**	−50.9 (−11.6)
insertion transition state	**7**	−40.4 (−1.1)
γ-agostic product	**8**	−55.4 (−16.1)
γ-agostic product	**8a**	−57.7 (−18.4)
β-agostic product	**9**	−63.2 (−23.9)
Chain Propagation: Path B (Reaction 3)		
hydrido-propylene complex	**10**	−25.7 (13.6)
β-agostic isopropyl complex	**11**	−40.8 (−1.5)
π-complex	**12**	−48.8 (−9.5)
insertion transition state	**13**	−37.8 (1.5)
γ-agostic product	**14**	−56.6 (−17.3)
β-agostic product	**15**	−63.8 (−24.5)
Chain Termination: β-Hydride Elimination (Reaction 4)		
$[L_2NiH]^+ + CH_2{=}CHCH_3$		12.9 (52.2)
Chain Termination: Hydrogenolysis (Reaction 5)		
reactants: $H_2 + [L_2NiCH_3]^+$	**1**	[0.0][c]
$(H_2)[L_2NiCH_3]^+$	**16**	[−11.4]
transition state for H−H activation	**17**	[−7.1]
product complex $(CH_4)[L_2NiH]^+$	**18**	[−19.6]
$CH_4 + [L_2NiH]^+$	**19**	[−4.1]
reactants: $H_2 + [L_2NiC_3H_7]^+$	**5**	{0.0}[d]
$(H_2)[L_2NiC_3H_7]^+$	**20**	{3.7}
transition state for H−H activation	**21**	{9.3}
product complex $(C_3H_8)[L_2NiH]^+$	**22**	{−3.9}
$(C_3H_8) + [L_2NiH]^+$		{14.6}

[a] Numbers given after slash include zero-point correction, while numbers given after // are the Gibbs free energies at 298.15 K and 1 atm. [b] Numbers given in parentheses are relative to the β-agostic complex **5**. [c] Numbers given in square bracket are relative to the $H_2 + [L_2NiCH_3]^+$ limit. [d] Numbers given in curly bracket are relative to the $H_2 + [L_2NiC_3H_7]^+$ limit.

(12) *GAUSSIAN94*. Frisch, M. J.; Trucks, G. W.; Schlegel, H. B.; Gill, P. M. W.; Johnson, B. G.; Robb, M. A.; Cheesemen, J. R.; Keith, T. A.; Petersson, J. A.; Montgomery, J. A.; Raghavachari, K.; Al-Laham, M. A.; Zakrzewski, V. G.; Ortiz, J. V.; Foresman, J. B.; Cioslowski, J.; Stefanov, B. B.; Nanayakkara, A.; Challacombe, M.; Peng, C. Y.; Ayala, P. Y.; Chen, W.; Wong, M. W.; Andres, J. L.; Replogle, E. S.; Gomperts, R.; Martin, R. L.; Fox, D. J.; Binkley, J. S.; DeFrees, D. J.; Baker, J.; Stewart, J. J. P.; Head-Gordon, M.; Gonzales, C.; Pople, J. A.; Gaussian Inc.: Pittsburgh, PA, 1995.

(13) Cui, Q.; Musaev, D. G.; Svensson, M.; Morokuma, K. *J. Phys. Chem.* **1996**, *100*, 10936.

(14) Musaev, D. G.; Morokuma, K., *Adv. Chem. Phys.* **1996**, *96*, 61.

γ-agostic interaction with the three $C^{\gamma}-H$ bond lengths of 1.113, 1.111, and 1.094 Å. In this γ-agostic complex, one should notice a long $C^{\beta}-C^{\gamma}$ bond distance of 1.567 Å compared with the normal CH_3-CH_2 distance of 1.505 Å at the same level of theory, suggesting a strong β-agostic interaction with the $C^{\beta}-C^{\gamma}$ bond. Actually the origin of the stability of this complex is more likely to be this C−C β-agostic interaction rather than C−H γ-agostic interaction.[15]

The γ-agostic product **4** can rotate the ethyl group around the $C^{\alpha}-C^{\beta}$ bond to form the β-agostic complex **5**. Although the transition state for this process was not located, previous studies for metallocenes and diimine−Pd(II) systems have indicated that the barrier for this $\gamma \rightarrow \beta$ agostic process is very small.[2,5] The β-agostic species, confirmed to be a real minimum, is 6.0 kcal/mol (without ZPC) below the γ-agostic complex. The $C^{\beta}-H$ bond involved in the β-agostic interaction in **5** is long, 1.197 Å, as much as 0.10 Å longer than 1.09 Å in the typical C-H bond. The $Ni-H^{agostic}$ distance of 1.719 Å is also very short and the Ni−C−C angle of 80.1° is small, indicating a very strong β-agostic interaction in **5**. The entire chain initiation reaction (1) to the β-agostic complex **5** is exothermic by 39.3 and 35.4 kcal/mol from the bare active catalyst **1** + ethylene, and 11.4 and 9.9 kcal/mol from the π-complex **2** calculated without and with ZPC, respectively. The rate-determining step in this initiation reaction is found to be the olefin insertion into the Ni−alkyl bond at TS **3**. This barrier calculated from the π-complex **2** is 9.9 and 10.7 kcal/mol without and with ZPC, respectively, and 11.7 kcal/mol with the Gibbs free energy.

The estimates of agostic interaction energies in **4** and **5** have been obtained as follows. We have optimized with C_1 symmetry a structure with no agostic interaction by placing the $C^{\alpha}-C^{\beta}$ bond *cis* to an Ni−N bond with *trans* staggered propyl conformation. Relative to this structure, **4** and **5** are lower by 8.3 and 14.3 kcal/mol, respectively, and these energies can be regarded as the net γ- and β-agostic interaction energies. These values are more or less what are expected for such interactions.

IV. Chain Propagation

The β-agostic complex **5** is an important intermediate from which the next step of polymerization process can proceed through a number of pathways. Because of the computational cost and expected similarities with the initiation step, no vibrational analysis has been performed for propagation and termination steps. We will at first study two chain propagation pathways.

Path A: Olefin Coordination and Insertion Leading to Linear Polymer Growth. There are two issues to be discussed before we perform any further calculation. First, Ziegler et al. have argued for zirconocene catalysts[16] that the β-agostic complex, **5**, has to rearrange the conformation of its alkyl chain to reach the α-agostic structure before the next olefin can effectively coordinate, and that a substantial barrier for this rearrangement constitutes the rate-determining step in the entire polymerization catalysis. However, Koga et al.[17] have shown clearly that the endothermic rearrangement and the strongly exothermic olefin coordination can take place simultaneously and there is no barrier between the β-agostic complex + olefin and the new olefin π-complex. Therefore, we did not try to find the transition state for this rearrangement/coordination process. Second, starting from the complex **5**, it is in principle possible that coordination and insertion of the next olefin takes place both from the frontside, i.e., at the $N-Ni-H^{\beta-agostic}$ quadrangle, or from the backside, i.e., at the $N-Ni-C^{\alpha}$ quadrangle. However, the backside attack is known to be quite unfavorable theoretically,[16] and thus it was not studied here.

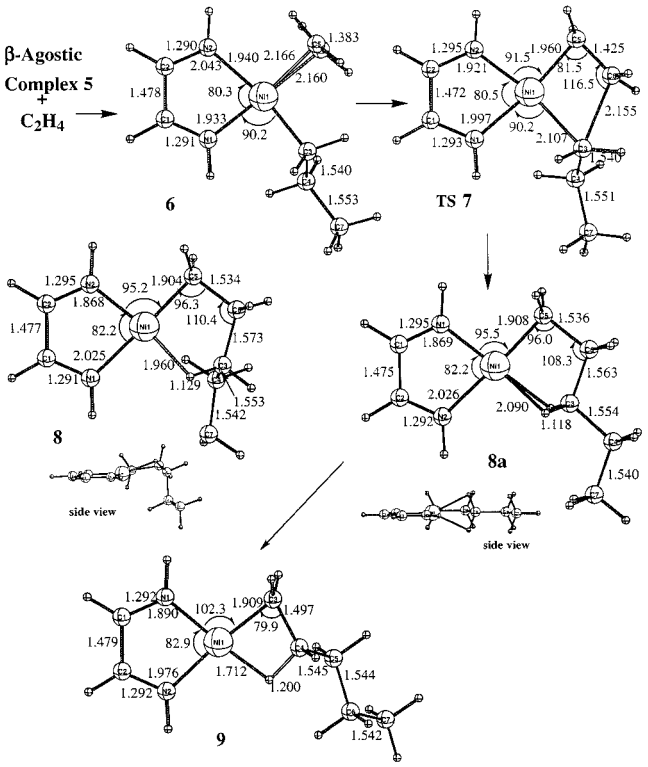

Figure 2. Optimized geometries (in Å and deg) of reactants, transition states and intermediates of the linear chain propagation step, path A (2): $[L_2M(CH_2CH_2CH_3)]^+ + CH_2{=}CH_2 \rightarrow [L_2M((CH_2CH_2)_2CH_3)]^+$.

For frontside attack, the olefin coordinates to the metal to form a new π-complex $[L_2M(CH_2CH_2)(CH_2CH_2CH_3)]^+$, (**6**), as shown in Figure 2. The structure of **6** is very similar to that of the corresponding π-complex, $[L_2M(CH_2CH_2)(CH_3)]^+$ (**2**), in the initiation step. The $Ni-C^{alkyl}$ distance in **6** is slightly longer than in **2**, suggesting that propyl is a slightly weaker ligand than methyl, and as a result, the $Ni-C^{olefin}$ distances are slightly smaller. Despite the shorter $Ni-C^{olefin}$ distances, the olefin coordination energy of 11.6 kcal/mol for **6** relative to the β-agostic complex **5** + C_2H_4 is much smaller (see Table 1) than 27.9 kcal/mol for **2** relative to the α-agostic complex **1** + C_2H_4. This energy difference can be understood by comparing the structures of reactants **1** and **5** on one side and π-complexes **6** and **2** on the other. While the olefin coordination to **1** does not cause a major geometry change in the reactant structure, the olefin coordination to **5** is accompanied by the disappearance of its β-agostic interaction, which should cause a substantial destabilization. Adding the β-agostic interaction of 14.3 kcal/mol estimated above to 11.6 kcal/mol, the real coordination energy for **6** is 25.9, which is not far from 27.9 kcal/mol for **2**.

Following the formation of the π-complex **6**, olefin insertion into the metal−alkyl bond occurs via transition state **7** leading to the γ-agostic product **8**. As seen in Figures 1 and 2, the transition states, **3** and **7**, corresponding to the insertion of the first olefin into the Ni−methyl bond and of the second olefin into the Ni−alkyl or (growing polymer), respectively, are very similar and are quite early as the olefin is only slightly activated. The barrier for this second insertion to form linear polymers is 10.5 kcal/mol, which is 0.6 kcal/mol higher than the barrier for the initiation step. This difference is likely to come from

(15) Koga, N.; Morokuma, K., *J. Am. Chem. Soc.* **1988**, *110*, 108

(16) Lohrenz, J. C. W.; Woo, T. K.; Ziegler, T. *J. Am. Chem. Soc.* **1995**, *117*, 12793.

(17) Koga, N. Presented in the Symposium on Computer Modeling of Polymerization Catalysts, Division of Polymeric Materials, 211th National Meeting of the American Chemical Society New Orleans, March 1996.

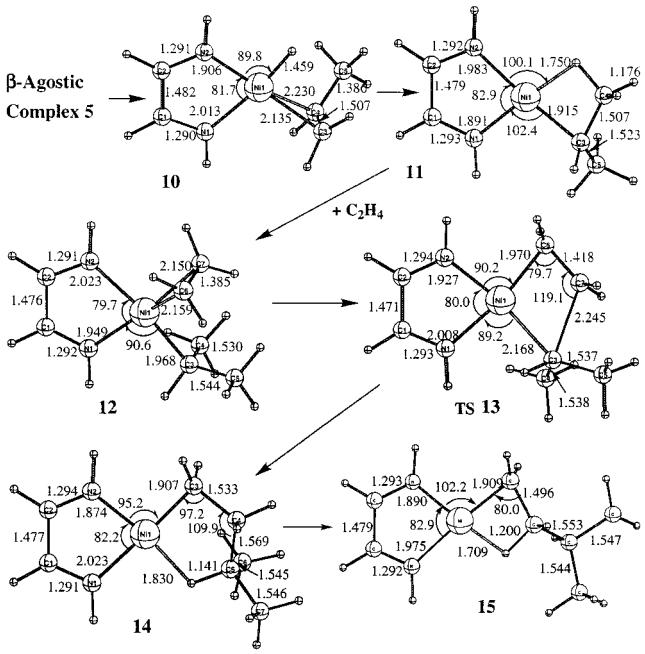

Figure 3. Optimized geometries (in Å and deg) of reactants, transition states, and intermediates of the branched chain propagation step path B (3): $[L_2M(CH_2CH_2CH_3)]^+ \rightarrow [L_2M(H)(CH_2{=}CHCH_3)]^+ \rightarrow [L_2M(CH(CH_3)_2)]^+$ (+ $CH_2{=}CH_2$) → $[L_2M(CH_2CH_2CH(CH_3)_2)]^+$.

the increased steric repulsion between the alkyl (polymer) chain and the catalyst for TS **7**. Two different conformations of γ-agostic products were found, one **8** with a single agostic interaction and the other **8a** with two agostic interactions. Here again, one can see not only long $C^{\gamma}-H$ bonds but also a long $C^{\gamma}-C^{\beta}$ bond suggesting the C−C β-agostic interaction as in **4**. The species with a single agostic interaction **8** is found to be higher in energy than the di-agostic species **8a** by 2.3 kcal/mol, presumably because of the steric repulsion between the long alkyl chain and the catalyst. The barrier between the two γ-agostic complexes corresponds to internal rotational around a C−C bond, and would be a few kcal/mol above the higher isomer. The lowest γ-agostic product **8a** is 18.4 kcal/mol lower in energy relative to **5** + C_2H_4.

In general, $[L_2M(CH_2CH_2)_2CH_3]^+$ product complexes may have several structures with α-, β-, γ-, δ-, and ϵ-agostic hydrogens. In a separate paper,[5] we have investigated all these complexes in more detail for the M = Pd case. It has been found that (i) the α-agostic complex does not exist; (ii) the β-agostic structure is energetically lower than γ-, δ-, and ϵ-agostic complexes by several kcal/mol, and their stability increases in the order: $\gamma < \epsilon < \delta \ll \beta$. Recently, similar results have been found by Lohrenz et al.[16] in studies of the butylbis(cyclopendadienyl)zirconium cation, $[Cp_2Zr(CH_2CH_2CH_2CH_3)]^+$. Therefore, the most stable conformation of $[L_2Ni(CH_2CH_2)_2CH_3]^+$ is the β-agostic complex which can be obtained by rotation around a C−C bond from the γ-agostic species **8** and **8a**. Our optimized β-agostic conformation of the $[L_2Ni(CH_2CH_2)_2CH_3]^+$, structure **9** in Figure 2, lies 5.5 kcal/mol below the lowest γ-agostic species **8a**. This energy lowering for the $\gamma \rightarrow \beta$ rearrangement in $[L_2Ni(CH_2CH_2)_2CH_3]^+$ is similar to the 6.0 kcal/mol value for $[L_2Ni(CH_2CH_2)CH_3]^+$ in the initiation step.

Path B: β-Hydride Elimination and Olefin Reinsertion Leading to Branched Polymer Growth. This path begins from the β-agostic complex **5,** and undergoes a β-hydride elimination via a transition state to reach the hydride−olefin species **10**, as shown in Figure 3 and Table 1. Despite substantial effort, the transition state between **5** and **10** could not be determined; the potential energy surface is very flat near the hydride−olefin complex **10** and the transition state is not expected to be more than 1 kcal/mol above **10**. This hydride−olefin complex **10** lies 13.6 kcal/mol above the β-agostic species **5**. The nearly perpendicular propylene in this π-complex can rotate and insert into the Ni−H bond at the other end of C=C double bond through a transition state with an anticipated low barrier to give the β-agostic isopropyl species **11**. This transition state for insertion could not be determined either, with an expected barrier from **10** of less than 1 kcal/mol. The entire region of the potential energy surface around **10** is extremely flat, as has been recognized before,[5] and the hydride−olefin complex **10** can effectively be considered as the transition state for β-hydride elimination and olefin reinsertion connecting the β-agostic *n*-propyl species **5** and the β-agostic isopropyl species **11**. The isopropyl isomer **11** is 1.5 kcal/mol lower in energy than the *n*-propyl isomer **5**.

The next olefin can now attack this new β-agostic species **11** leading to a π-complex **12** which is 8.0 kcal/mol more stable than **11** + C_2H_4. An insertion transition state **13** leads from the π-complex **12** to the γ-agostic product **14** with branched polymer growth. The barrier for this process of 11.0 kcal/mol is similar to the 10.5 kcal/mol for the insertion of the second olefin via path A for linear polymer growth. The γ- and β-agostic branched isomers are similar in energy to their linear counterparts. The β-agostic branched isomer **15** is 7.2 kcal/mol lower in energy than the γ-agostic species **14**.

V. Chain Termination

A number of possible chain termination processes have been reported[1,2,16] for metallocene based catalytic processes including β-hydride transfer, alkene C−H bond activation by metal−alkyl complexes, H-exchange between alkyl and olefin fragments of the metal alkyl olefin complexes, and hydrogenolysis. In our separate paper,[5] all of these possible chain termination processes have been investigated in more detail for the Pd(II)-catalyzed ethylene polymerization reaction. There we have found that H-exchange and alkene C−H bond activation processes are inefficient chain termination processes due to very high activation barriers. Therefore, we will not study these processes here, but concentrate on β-hydride transfer and hydrogenolysis chain termination mechanisms for the Ni(II)-catalyzed olefin polymerization.

The β-hydride transfer process has been discussed in an earlier section. It has been shown that β-hydride transfer from the β-agostic alkyl complex **5** proceeds nearly straight uphill with a small reverse barrier to the hydride−olefin species **10** which is 13.6 kcal/mol higher in energy. By reinsertion of the olefin in **10** with opposite regiochemistry, as shown as path B in Scheme 1, a branched polyethylene will be formed. If the dissociation of propylene (or a polymer with a terminal olefin) takes place from **10**, the polymerization chain is transferred, as shown as path C in Scheme 1. In other words, the current polymer chain will be terminated with the production of a polymer with a terminal olefin and a new chain will be initiated with the newly formed metal−hydride species. As shown in Table 1, the dissociation of propylene from the olefin−hydride intermediate **10** is 38.6 kcal/mol endothermic in the gas phase, producing a hydride complex $[L_2NiH]^+$. In solution, the solvation would make this process much less endothermic. For instance, the coordination energy of ethylene to the hydride is only 4 kcal/mol smaller than that of propylene for the corresponding Pd complex.[5] If we assume this difference for Ni, then this dissociation and coordination process would be endothermic only by 4 kcal/mol. However, this *dissociative*

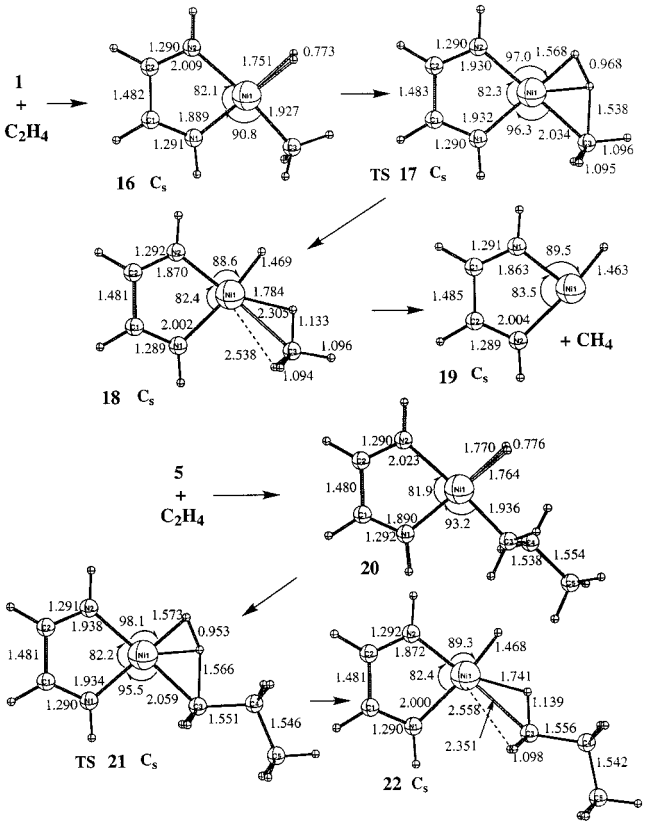

Figure 4. Optimized geometries (in Å and deg) of reactants, transition states, and intermediates of the chain termination hydrogenolysis step (5): $[L_2MR]^+ + H_2 \rightarrow [L_2M(H_2)R]^+ \rightarrow [L_2MH]^+ + HR$ for R = CH_3 and $CH_2CH_2CH_3$. Label C_s indicates that C_1 optimization converged to a C_s structure.

termination pathway cannot compete with the chain propagation path B, which also starts from **10** with an exothermicity of 15.1 kcal/mol for reinsertion.

It should be noted that the *associative displacement* mechanism suggested by Brookhart and co-workers[3] where the coordinating olefin exchanges with ethylene from the solution, is likely to be one of the preferable chain transfer mechanisms. This mechanism assumes the existence of a stable five-coordinated bis(olefin) complex or a low energy transition state for the olefin exchange reaction. Our preliminary calculations suggest the existence of the former. Because of its potential importance in the chain termination process, we will study the associative displacement mechanism in detail in our upcoming paper.

Hydrogenolysis is another chain termination process accessible when there is enough hydrogen pressure. We examined this for the addition of a hydrogen molecule to $[L_2Ni\text{-}CH_3]^+$ **1** and to the β-agostic propyl species $[L_2Ni\text{-}CH_2CH_2CH_3]^+$ (**5**). As depicted in Figure 4, the dihydrogen complexes, **16** and **20**, are formed first, with H−H and Ni−H bond distances of 0.77−0.78 Å and 1.75−1.77 Å, respectively. The next step is the activation of the H−H bond which occurs via four-center metathesis-like transition states, **17** and **21**, respectively. In these transition states, the H−H bond has been stretched to 0.968 and 0.953 Å and the Ni−C bond stretched to 2.03−2.06 Å, while the forming C−H and Ni−H bond distances are reduced to 1.54−1.57 Å and 1.57 Å, respectively. As seen in Figure 4, the products **18** and **22** are ion−molecule complexes where the transition metal center is coordinated with the alkane molecule via its three hydrogen atoms (one in particular).

Concerning the energetics (Table 1) for the methyl species **1**, the dihydrogen complex **16** is stable relative to the dissociation limit (**1** + H_2) by 11.4 kcal/mol. However, for the β-agostic propyl species **5**, the dihydrogen complex **20** lies 3.7 kcal/mol higher than **5** + H_2, and is only kinetically accessible from **5** + H_2. The structure of **20** indicates that the β-agostic interaction is completely lost and it may better be considered to be formed from the non-agostic structure. Relative to the non-agostic structure discussed in a preceding section, **20** is more stable by 10.6 kcal/mol, nearly comparable to 11.4 kcal/mol for **16**. The transition state separating the dihydrogen complex **20** from **5** + H_2 is extremely small, and we could not determine its structure. The activation barriers at **17** and **21** for the rate-determining H−H activation from the dihydrogen complexes **16** and **20** to give the hydride−alkane product complexes L_2NiH^+-CH_4, (**18**) and L_2NiH^+-C_3H_8 (**22**) are 4.3 and 5.6 kcal/mol, respectively, and hydrogenolysis should be an easy termination process if there is enough hydrogen pressure. Products **18** and **22** are 19.6 and 3.9 kcal/mol lower than reactants, **1** + H_2 and **5** + H_2, respectively. The dissociation processes for the **18** → $L_2NiH^+ + CH_4$ and **22** → $L_2NiH^+ + C_3H_8$ are endothermic by 15.5 and 18.5 kcal/mol, respectively, in the gas phase, but this process can take place easily in solution, where another ligand, most likely ethylene, will replace the alkane.

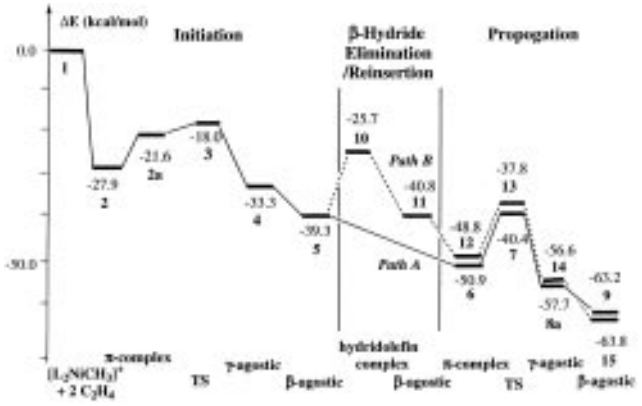

Figure 5. The potential energy (without ZPC) profile of the $[L_2NiCH_3]^+$-catalyzed ethylene polymerization reactions, including the chain initiation step (1), the linear chain propagation step, path A (2), and the branched chain propagation step, path B (3).

VI. Comparison of Different Mechanisms of the Ni(II)-Catalyzed Olefin Polymerization Reaction

In Figure 5, the potential energy profile of the entire diimine−Ni-catalyzed ethylene polymerization reaction is presented. The insertion of ethylene into the Ni−alkyl bond from the alkyl olefin π-complexes **2**, **6**, and **12** is the rate-determining step for both initiation and propagation reactions. Therefore, one may conclude that the alkyl olefin complexes are the resting states in the catalytic cycle, which is in agreement with experimental findings.[3] The insertion barrier is 9.9 kcal/mol at **3** for the initiation step, and slightly increased to 10.5 and 11.0 kcal/mol for subsequent insertions reactions at transition states **7** and **13** leading to linear (path A) and branched (path B) propagation products, respectively. The difference in the activation barrier between the linear and branched propagation processes, 0.5 kcal/mol, is so small that this difference cannot be the discriminating factor between linear and branched polymer growth. This point will discussed again later.

Passage over the insertion transition state and reorganization of the growing polymer chain conformation leads to β-agostic complexes **5**, **9**, and **15**. The entire reaction $L_2NiR^+ + C_2H_4 \rightarrow [L_2Ni(CH_2CH_2R)]^+$ is exothermic by 39.3 kcal/mol for the initialization step 1, R = CH_3, and the exothermicity of the

subsequent linear and branched propagation reactions 2 and 3, R = C_3H_7, decreases to 23.9 and 24.5 kcal/mol, respectively. This difference in the exothermicity between the initiation reaction and the propagation reactions has been explained above in terms of the absence of β-agostic interactions in the reactant of the former, $L_2NiCH_3^+$ **1**; one does not have to break the β-agostic interaction during the reaction.

The β-agostic complexes **5**, **9**, and **15** are important points on the potential energy surface, where the reaction can split into two different pathways for linear (path A) and methyl-branched (path B) growth. For instance, for **5** as discussed above, path A starts by frontside coordination of ethylene with an energy gain of 11.6 kcal/mol. However, **5** may also initiate the first step of path B by elimination of the β-agostic hydride with a barrier of *ca.* 14−15 kcal/mol to give a hydride-olefin species **10**, which is 13.6 kcal/mol above **5**. Complex **10** can rotate and reinsert the olefin with a different regiochemistry to give the branched alkyl−Ni complex, **11**. The rotation/reinsertion **5** → **11** is exothermic by 1.5 kcal/mol. The resultant alkyl complex **11** has an empty site and binds another olefin to give a new olefin alkyl complex, **12,** with an energy gain of 8.0 kcal/mol, and growth of a branched polymer is initiated. The entire process of **5** → **12** is exothermic by 9.5 kcal/mol. Though we used **5** in the above discussion as a representative of the key species where two paths will split, the path can split also at the other β-agostic complexes **9** and **15**, providing complicated sequences of linear and branched polymer growth.

Thus, as seen in Figure 5, path A is a bimolecular ethylene coordination reaction without barrier from the β-agostic complex **5** to π-complex **6**, followed by a unimolecular migratory insertion with an *ca.* 10 kcal/mol barrier, while path B involves an initial unimolecular reaction with a 14−15 kcal/mol β-hydride activation barrier from **5** to **12**, followed by essentially the same bimolecular and unimolecular sequence as in path A. Therefore, one should expect that the Ni(II)-catalyzed ethylene polymerization reaction will produce more linear than methyl-branched polymer growth under normal conditions, which is in excellent agreement with experiment.[3] If we simply assume that the difference of 4 kcal/mol determines the branching ratio, one expects that branching occurs 1 in 1000. This is slightly too small in comparison with experiment where branching occurs 6 in 1000 ($\Delta\Delta G^{\ddagger}$ = 0.3 kcal/mol), suggesting that a higher level of theory would be able to estimate this difference quantitatively. The ratio of the linear/branched growths should depend on external factors such as temperature and ethylene pressure, as well as internal factors such as the nature of the ligands and the metal atom. A higher temperature should facilitate path B and, consequently, result in more methyl-branched growth. On the other hand, higher ethylene pressure will result in more linear growth. These qualitative conclusions also are in excellent agreement with experimental findings.[3]

VII. Comparison of the Mechanisms of Ethylene Polymerization Reactions between Diimine−Ni and Zirconocene Catalysts

As mentioned in the Introduction, metallocene catalyzed ethylene polymerization reactions have been a focus of intensive investigations over the last several years, and numerous interesting results have been accumulated.[1,2,16−18] Here, we will compare our theoretical results presented above for the diimine−Ni(II) catalyzed ethylene polymerization reaction with those for zirconocene catalyzed ethylene polymerization. At first, let us very briefly summarize the theoretical results for the polymerization reaction catalyzed by methylbis(cyclopentadienyl)-zirconium, $[ZrCp_2CH_3]^+$, reported in the literature[1,2] and obtained by us[18] at the same level of theory as used in this paper.

1. The reaction involves the coordination of an olefin to form a π-complex, followed by olefin insertion into the Zr−C_α bond via a four center transition state to form the direct product, the γ-agostic complex. Then the γ-agostic complex rearranges into a more stable β-agostic complex with a few kcal/mol rotational barrier. The olefin coordination energy, the insertion barrier relative to the π-complex, and the exothermicity of the chain initiation step are 20−23, 7−8, and 30−33 kcal/mol for the active catalyst $[(CpXCp)ZrCH_3]^+$ where the bridge X connecting two Cp rings is X = CH_2, SiH_2, and C_2H_4 or without connection. The β-agostic complex possesses a vacant coordination site and serves as the starting point for the next insertion step and consequently produces linear polymers.

2. Since β-hydride elimination takes place with a significant (15−20 kcal/mol) activation barrier, methyl-branched polymer growth seems to be less probable.

3. Four chain termination processes have been studied: β-hydride elimination, C−H activation, H-exchange, and hydrogenolysis. From both a kinetic and thermodynamic perspective, C−H activation, H-exchange, and hydrogenolysis are favored as the prevailing chain terminating mechanisms.

The comparison of the above-mentioned findings for zirconocene catalysts with those obtained in this paper for diimine−Ni(II) catalyst shows the following similarities and differences.

1. The mechanism of the chain initiation reaction (1) and the linear chain propagation reaction (2) for the Ni(II) catalyst is similar to that for the zirconocene catalyst. It includes the coordination of ethylene to the metal center, the insertion of the olefin into the metal−alkyl bond, and the formation of a γ-agostic product with a small barrier which rearranges to a more stable β-agostic product. However, there are differences in the calculated energetics of these processes.

At first, the calculated coordination energy of ethylene for Ni systems is about 5−6 kcal/mol larger than that for zirconocene systems. Since the active catalyst L_2NiR^+ is solvated in solution, this energy difference may be irrelevant to the initial kinetics. Nonetheless, the difference in the Cp_2ZrR^+-C_2H_4 and L_2NiR^+-C_2H_4 binding energies can be explained by the nature of the M−olefin bond. Usually M−olefin bonding consists of two components: the σ-component resulting from donating the electron density from the π-orbital of the olefin into the empty sd_σ-orbital of the metal, and the π-component resulting from back-donation of the electron density from the d_π orbital of the metal to the π*-orbital of the olefin. Since early transition metals like Zr have no occupied d_π orbital, there will be no back-donative contribution. Late transition metals like Ni can form a bond with olefin with both donation and back-donation making a substantial contribution.

Second, the rate-determining barrier for Ni(II)-catalyzed olefin insertion, 9−11 kcal/mol, is a few kcal/mol larger than that for zirconocene-catalyzed insertion. Thus, zirconocene-catalyzed ethylene polymerization should take place slightly faster than Ni(II)-catalyzed ones at the same experimental conditions.

2. Another interesting comparison between zirconocene- and Ni(II)-catalyzed ethylene polymerization can be found for the β-hydride elimination process. As mentioned above, the activation barrier for β-hydride elimination is high for both catalysts but is higher (15−20 kcal/mol) for zirconocene than for Ni(II) (14−15 kcal/mol). The origin of this difference may be attributed to the above mentioned difference in L_2ZrR^+−

(18) Froese, R. D. J.; Das, P. K.; Musaev, D. G.; Lauffer, D.; Morokuma, K. In preparation.

olefin and Cp_2NiR^+−olefin interactions. During this process, the β-agostic metal−alkyl complex is converted into a metal−hydride−olefin complex; the stronger metal−olefin interaction in the Ni(II) system would stabilize the transition state and the intermediate and, consequently, facilitate the whole process.

Since the β-hydride elimination/reinsertion process has a high barrier for both systems, one would expect that the linear polymer growth process is preferred over branched growth. In the Ni(II) systems, the barrier height for branched growth is only *ca.* 4−5 kcal/mol higher than that for linear growth, whereas this difference is substantially larger (8−10 kcal/mol) for the zirconocene system. Thus one would expect that the Ni(II) system produces more branches than the zirconocene system.

3. Hydrogenolysis is found to be an efficient chain termination process in the presence of hydrogen both in the diimine−Ni and zirconocene systems.

VIII. Conclusions

From the present research, the following conclusions could be drawn.

1. The chain initiation reaction (1) starts from the coordination of ethylene to the metal center, followed the insertion of an olefin into metal−alkyl bond leading to the formation of a γ-agostic product which with a small barrier rearranges to a more stable β-agostic product **5**. The ethylene coordination energy, the insertion barrier relative to the more stable π-complex, and exothermicity of the entire reaction (1) are calculated to be 25.5, 10.7, and 35.4 kcal/mol with ZPC, respectively. The corresponding Gibbs free energies at 298.15 K are 14.9, 11.7, and 24.2 kcal/mol, respectively.

The β-agostic complex **5** (as well as its equivalents in subsequent propagation steps) is an important point on the potential energy surface of the entire process. From this point, the reaction splits into two different channels leading to linear (path A) or methyl-branched (path B) polymer growth. For path A, reaction 2 starts by frontside attack of ethylene to the β-agostic complex **5** which takes place with complexation energy of 11.6 kcal/mol. Then an olefin inserts into the $Ni^+-CH_2CH_2CH_3$ bond with a 10.5 kcal/mol barrier. Overcoming this barrier leads to a linear growth product, the β-agostic $[L_2Ni(CH_2CH_2)_2CH_3]^+$. The first step of path B is the activation of the β-agostic C−H bond with a 14−15 kcal/mol barrier which leads to a hydride olefin species **10**. Complex **10** via rotation and reinsertion rearranges into $[L_2Ni(CH(CH_3)_2)]^+$ (**11**). The resultant branched alkyl complex **11** coordinates the next olefin giving a new olefin alkyl complex, **12**, with an energy gain of 8.0 kcal/mol. Then the insertion of the olefin into the $L_2Ni^+-CH(CH_3)_2$ bond takes place with a 11.0 kcal/mol barrier resulting in β-agostic $[L_2Ni(CH_2CH_2CH(CH_3)_2]^+$ (**15**) with a methyl-branched growing polymer.

2. The rate-determining step of the entire polymerization reaction is the insertion of the olefin into the L_2Ni^+- alkyl bond from an olefin π-complex. The activation energies without ZPC are 9.9 (10.7 with ZPC, and 11.7 for Gibbs free energy), 10.5, and 11.0 kcal/mol for chain initiation, linear chain growth, and branched chain growth, respectively. The olefin alkyl complexes are the resting states in the catalytic cycle, which is in agreement with the experimental findings.

3. Paths A and B which start from the β-hydride complex **5** to an olefin complex are exothermic by 11.6 and 9.5 kcal/mol, respectively. Path A, a simple bimolecular coordination reaction, proceeds without energetic barrier, while path B is preceded by a unimolecular reaction of a 14−15 kcal/mol β-hydride activation barrier before a no-barrier bimolecular coordination reaction. Therefore, one should expect that the Ni(II)-catalyzed ethylene polymerization reaction will produce more linear than methyl-branched polyethylenes under normal conditions. However, the ratio of the linear/branched growths is expected to depend on external factors such as temperature, ethylene pressure, and steric factors, as well as internal factors, i.e., the nature of the ligands and the metal atom. Increased temperature should facilitate the activation process, path B, and consequently, result in more methyl branches. On the other hand, an increase in ethylene pressure will favor the bimolecular process, path A, and more linear polymers. These conclusions are in excellent agreement with experimental findings.[3]

4. A termination process can be initiated from the intermediate L_2NiH^+−propylene **10**, which is the result of β-hydride activation discussed above, as shown as path C in Scheme 1. Since the branched chain propagation, path B, starts from the same complex **10** and has a relatively small insertion barrier of 11.0 kcal/mol, the chain termination via *dissociative* elimination of polyethylene with a terminal olefin, which is 38.6 kcal/mol endothermic, cannot compete with propagation. However, the *associative displacement mechanism* suggested by Brookhart and co-workers,[3] where the coordinating polymer is associatively replaced by ethylene from the solution, is more likely to be one of the preferable chain transfer mechanisms.

The other prevailing chain terminating process in the diimine−Ni-catalyzed olefin polymerization reaction is hydrogenolysis, reaction 5, which proceeds via (i) coordination of the hydrogen molecule to the metal center of L_2NiR^+ giving a dihydrogen complex, (ii) activation of H−H and formation of C−H bonds, and (iii) elimination of an alkane molecule resulting in a diimine−nickel−hydride complex. The coordination of the H_2 molecule to the Ni center is exothermic by 11.4 kcal/mol for $R = CH_3$, while it is endothermic by 3.7 kcal/mol for $R = C_3H_7$. In the next step, the activation of the H−H bond and the formation of the C−H bond takes place through a four-center transition state with 4.3 and 5.6 kcal/mol energetic barriers for $R = CH_3$ and C_3H_7, respectively, relative to the corresponding dihydrogen complexes. The entire reaction $L_2NiR^+ + H_2 \rightarrow L_2PdH^+ + RH$ is exothermic by 4.1 kcal/mol for $R = CH_3$ but is endothermic by 14.6 kcal/mol for $R = C_3H_7$.

5. A comparison of the diimine−Ni(II)-catalyzed ethylene polymerization reaction with the zirconocene-catalyzed one shows that (a) the zirconocene-catalyzed polymerization should take place slightly faster than the Ni(II)-catalyzed one at the same experimental conditions; (b) the preferable chain growth reaction for both systems is the bimolecular reaction leading to linear polyethylenes. The Ni(II) catalyst should produce more branches than zirconocene.

Acknowledgment. The use of the computational facilities and programs at the Emerson Center is acknowledged. The present research is in part supported by grants (CHE-9409020 and CHE96-27775) from the National Science Foundation. R.D.J.F. acknowledges a postdoctoral fellowship from the Natural Sciences and Engineering Research Council of Canada. M.S. acknowledges a postdoctoral fellowship from the Swedish Natural Science Research Council.

JA9628314